University of Groningen

Breaking the interface

Metzler, Lukas; Rehbein, Ulrike; Schönberg, Jan-Niklas; Brandstetter, Thomas; Thedieck, Kathrin; Rühe, Jürgen

IMPORTANT NOTE: You are advised to consult the publisher's version (publisher's PDF) if you wish to cite from it. Please check the document version below.

Document Version
Publisher's PDF, also known as Version of record

Link to publication in University of Groningen/UMCG research database

Breaking the Interface: Efficient Extraction of Magnetic Beads from Nanoliter Droplets for Automated Sequential Immunoassays

Lukas Metzler,[⊥] Ulrike Rehbein,[⊥] Jan-Niklas Schönberg, Thomas Brandstetter,* Kathrin Thedieck,*,[#] and Jürgen Rühe*,[#]

ACCESS | 📊 Metrics & More | 📰 Article Recommendations | 🆘 Supporting Information

ABSTRACT: Droplet-based microfluidic systems offer a high potential for miniaturization and automation. Therefore, they are becoming an increasingly important tool in analytical chemistry, biosciences, and medicine. Heterogeneous assays commonly utilize magnetic beads as a solid phase. However, the sensitivity of state of the art microfluidic systems is limited by the high bead concentrations required for efficient extraction across the water−oil interface. Furthermore, current systems suffer from a lack of technical solutions for sequential measurements of multiple samples, limiting their throughput and capacity for automation. Taking advantage of the different wetting properties of hydrophilic and hydrophobic areas in the channels, we improve the extraction efficiency of magnetic beads from aqueous nanoliter-sized droplets by 2 orders of magnitude to the low μg/mL range. Furthermore, the introduction of a switchable magnetic trap enables repetitive capture and release of magnetic particles for sequential analysis of multiple samples, enhancing the throughput. In comparison to conventional ELISA-based sandwich immunoassays on microtiter plates, our microfluidic setup offers a 25−50-fold reduction of sample and reagent consumption with up to 50 technical replicates per sample. The enhanced sensitivity and throughput of this system open avenues for the development of automated detection of biomolecules at the nanoliter scale.
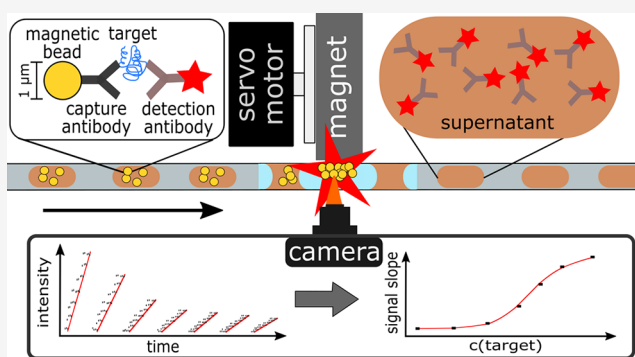
Increasingly, droplet-based microfluidics is being recognized as a powerful tool for the analysis of biological samples. This technology offers multiple options to implement high throughput setups with a high degree of automation for analyses at the microscale. Hundreds to thousands of uniform aqueous droplets are employed to serve as individual microreactors for (bio)chemical assays.[1,2] The droplets are created at T-junctions, or more complex geometries, at which an aqueous solution joins an immiscible oil. Due to surface instabilities, the aqueous solution is sheared off into individual droplets carried downstream by the water-immiscible continuous phase.[3] The volume of the droplets is typically in the femto to nanoliter range, enabling assays with minimal sample consumption.[1,4] Multiple operations to manipulate the droplets, including merging, mixing, splitting, and sorting, have been established and are frequently used for the implementation of state of the art immunoassays in microfluidics.[4−6] Thus, assay components can be added to individual droplets, and droplets carrying features of interest can be selected for analysis. If the droplets' dimensions are confined by the channel dimensions, they are often referred to as plugs.[7]

The implementation of biochemical assays in one homogeneous, liquid phase without intermittent washing steps has been well established for droplet microfluidics.[4,8] In contrast, heterogeneous assays allow the separation of the assay products from the unbound components which usually increases the sensitivity and specifity of an assay. On microtiter plates, repeated washing steps can be easily implemented by exchanging the liquid phase while performing immunoblots, enzyme-linked immunosorbent assays (ELISA), or fluorescence-based sandwich immunoassays. Therefore, they remain commonly used analysis methods, both in research and clinical analytics. However, in droplet-based approaches the separation of the assay product from the unbound components remains challenging. Overcoming this hurdle would be of great benefit for the field of analytical chemistry, especially when sample volumes and reagents are limited and high throughput is required.

In two-phase flow setups, functionalized magnetic beads are frequently used as a solid phase for heterogeneous affinity assays. They promise easy purification and isolation of the assay product from the aqueous reaction environment for
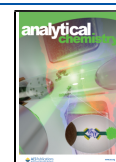
Figure 1. Illustration of the fluorescence-based sandwich immunoassays on magnetic beads in nanoliter droplets. The sample(s) (flow 2, shades of blue) and the detection antibody (flow 3, 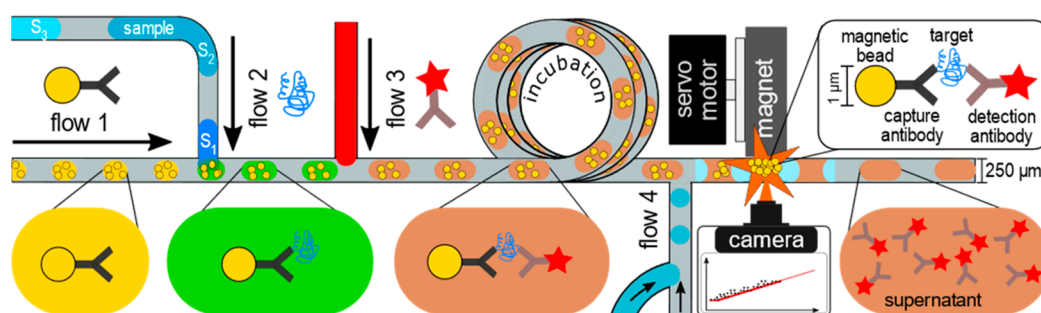red) are added successively to a droplet train containing magnetic beads (flow 1, yellow). During incubation, the droplets move through the fluidic channel. A final wash step takes place at the magnetic trap, where the magnetic beads are separated from the supernatant. The accumulation of the fluorescence signal is recorded with an inverted microscope. Flow 4 aids to release of captured beads.

downstream analysis.[9] However, magnetic bead extraction from aqueous droplets is limited by the high surface tension of the water–oil interface. As the efficiency of magnetic bead extraction is a key determinant of sensitivity in microfluidic systems, optimizing the bead extraction represents a potent means to enhance their performance.

One way to overcome this challenge is to avoid extraction altogether. This can be achieved by merging the aqueous droplets with the continuous aqueous phase, thus avoiding the need for particles to pass through the water–oil interface.[10] This strategy enables the analysis of low amounts of beads at the expense of losing the droplets in the continuous phase. This approach, however, excludes the option to analyze the droplet phase after the extraction or to reuptake the magnetic beads into another droplet. To maintain the droplets' integrity, several studies have proposed droplet splitting to enrich the assay product. Therefore, droplets are divided at a T-junction, while steering the beads by magnetic force into one of the daughter droplets.[11−13] Even though this approach does reduce background signals from molecules dissolved in the aqueous phase, this concept by definition suffers from substantial residual contamination from the initial liquid phase.[12,13]

In spite of its shortcomings, magnetic bead extraction from the droplets still appears more promising than the afore-mentioned alternatives, as the major fraction of the liquid in the droplet is removed, and only residual amounts of the initial aqueous phase remain trapped between the closely packed magnetic beads.[14] Conceptually, this approach requires the extraction of the beads with the bound analyte by piercing the water–oil interface. In 2012, Ali-Cherif et al.[14] demonstrated an effective extraction of almost pure magnetic beads from nanoliter droplets. Magnetic coils with sharp tips served to focus the magnetic field and thereby enhance the magnetic force acting on the magnetic bead clusters.[14,15] For this kind of magnetic trap, a magnetic bead concentration of at least 1−10 mg/mL is required[14,16−18] to obtain the minimal cluster size that overcomes the interfacial barrier. While the magnetic force (F_M) and the mass (m) of an object scale with the size (d) in a cubic relation ($F_M \sim m \sim d^3$), the surface tension (γ) scales with d in a linear manner ($\gamma \sim d^1$).[19] At low concentrations, only small bead clusters are formed, and thus, the surface tension exceeds the magnetic force. This prevents successful extraction of small bead quantities. Increasing the bead concentration, however, is not advantageous as the number of detectable molecules per bead decreases, whereas the

increased number of beads results in a higher background signal and variance due to higher autofluorescence and/or light scattering. Both factors usually lead to an increase in the lower limit of detection (LoD).

To aid the transit through the water–oil interface, we previously suggested to add nonfunctionalized magnetic beads prior to the extraction of functionalized beads.[20] This strategy allows for the concentration of analyte molecules onto a small number of particles but still suffers from the need of a relatively large amount of beads at the point of detection—creating a substantial background signal. Furthermore, the additional step required prior to magnetic bead extraction hampers automation. Another concept to aid the breakup of the water–oil interface is the wetting of a hydrophilic channel by the aqueous phase.[21] This removes the interface between the droplet and the channel and thus reduces the force necessary to drag the magnetic particles to the channel wall. Schönberg et al.[22] demonstrated the potential to extract magnetic beads down to concentrations of 1 μg/mL while preserving the droplets' integrity. However, the compatibility of this concept with microfluidic immunoassays remains to be tested.

In this study, we describe a microfluidic setup that allows for the extraction of magnetic beads at low concentrations. We develop and validate the application for heterogeneous sandwich immunoassays at the nanoliter scale. To capture and release magnetic beads, we introduce a magnetic trap that allows us to switch the local magnetic field on and off. We determine the influence of the assay parameters on the analytical performance, in particular, on the limit of detection (LoD).

■ CONCEPT AND OPERATING PRINCIPLE

Microfluidic Immunoassay. We base our microfluidic platform on the setup developed by Rendl et al.,[20] in which heterogeneous assays are performed in plugs serving as miniaturized reaction compartments. The system consists of perfluorinated tubings filled with perfluorocarbon carrier oil (FC-43 or FC-3283) and reagents in aqueous solution. The tubings are connected through T-junctions at which the aqueous solution flowing in becomes sheared off into the water-immiscible carrier oil, thereby forming nanoliter droplets. While the setup of Rendl et al.[20] consisted of one T-junction through which different reagents were added by repeated forward and backward flows, we combine here two T-junctions (Figure 1). This allows us to reduce the droplet movements to a minimum. First, we add an aqueous dispersion

of magnetic beads coated with capture antibodies to the carrier oil, thereby generating plugs in reverse direction to flow 1 (Figure 1, yellow). After lining up of the plugs this way, the analyte containing sample(s) and detection antibodies are added to the plugs at the two T-junctions (Figure 1, flow 2 [blue] and 3 [red]). The flow speed is kept constant after the last merging step so that the incubation time is equal for each droplet immunoassay.

To setup and optimize this microfluidic system, a simplified assay with streptavidin and Atto-647N-Biotin (Atto-Biotin) was used. The streptavidin–biotin binding is the strongest known noncovalent interaction between biological molecules ($K_D = 10^{-13}$ M).[23] This strong affinity allowed for optimization of the performance of the microfluidic system. Thus, plugs with streptavidin-coated beads (flow 1) were merged with Atto-Biotin containing samples at the first T-junction (flow 2) and PBST (phosphate-buffered saline with 0.1% (v/v) Tween 20) at the second T-junction (flow 3). The latter was used for addition of detection antibody for sandwich immunoassays (see below, proof of concept).

The magnetic trap is a key feature of this microfluidic platform. For detection, the magnetic beads, carrying the assay product, must be extracted from the plugs, while the supernatant with unbound analyte and antibodies moves downstream. To this, two neodymium magnets were placed at either side of the tubing to capture the beads at the point of detection (marked by a orange star in Figures 1 and 2a). The
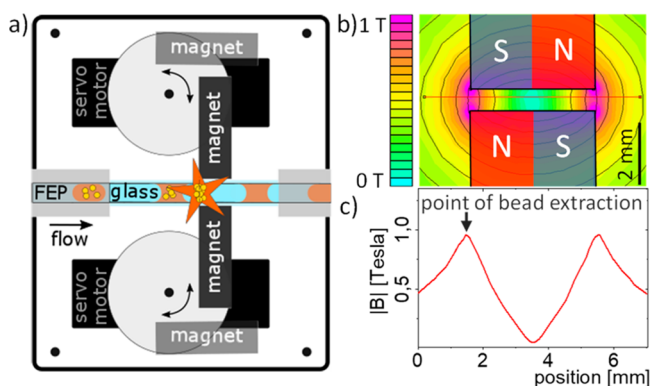
Figure 2. Magnetic trap. (a) Illustration of the magnetic trap for extraction of beads (yellow) from aqueous droplets (brown). Beads are kept stationary at the point of extraction/detection (orange star) by two servomotor-controlled magnets. FEP, fluorinated ethylene propylene tubing. (b) Simulation of the magnetic field lines for the two magnets in the magnetic trap. N, magnetic north. S, magnetic south. T, Tesla. (c) Simulated intensity of the magnetic field along the fluidic channel [red line in (b)]. The bead extraction takes place at the first maximum of the magnetic field. Arrow, point of bead extraction.

two magnets are arranged such that they generate a magnetic field B, focused at the magnet edges (B_{max} = 1 T, Figure 2b [pink area] and 2c [max. values on y-axis]). This two-magnet setup maximizes the gradient of the magnetic field and led to a well-defined area of extraction at the first peak of the magnetic field (Figure 2c) The position of the magnets is controlled by servomotors (Figure 2a) actuated by a programmable Arduino microcontroller. This allows for the synchronization of the magnetic trap to the flow pattern and can automatically open the magnetic trap after each measurement. Thus, the trapped beads can be released from the point of extraction, and

subsequent droplets clear the tubing. An additional wash flow (Figure 1, flow 4) can further aid the release of the beads.

It is assumed that all the plugs carry the same average fluorophore load (i.e., fluorescent assay product). Therefore, as these fluorophores accumulate in the magnetic trap, a linear increase of the detection signal is expected. Thus, a linear regression can be used to evaluate the mean contribution of the droplets to the signal. In other words, the slope of the signal increase correlates to the amount of fluorescent assay product at the surface of the beads.

■ MATERIALS AND METHODS

Functionalization of Beads with Capture antibodies. The streptavidin-coated superparamagnetic beads (Dynabeads MyOne Streptavidin T1, #65601, Invitrogen, US) were functionalized with the biotinylated capture antibodies as recommended by the supplier (IL-6: antibody raised in goat against human IL-6, residues M1–M212, #BAF206, R&D, US; mTOR: Clone 3G6,[1] antibody raised in rat against human mTOR, residues T221–I260). The magnetic beads were washed twice with PBST and diluted to a concentration of 0.1 mg/mL. Capture antibodies were added in amounts exceeding the binding capacity of the beads and incubated for at least 30 min at room temperature with gentle agitation. Unbound antibodies were removed by three washes with PBST. Beads were reconstituted in PBST to the final concentration.

Microfluidic Procedure. The procedure consists of the following steps: (i) droplet generation in reverse direction to flow 1 (see Figure 1), (ii) addition of further reagents to the droplets at the T-junctions: merging with droplets containing sample and fluorophore-labeled detection antibodies or PBST (in the case of Atto-Biotin experiments), (iii) incubation at a constant flow rate; incubation times: Atto-Biotin experiments, t = 13.5 min; sandwich immunoassays, t = 27 min, and (iv) magnetic bead extraction and detection of the fluorescent signal at the magnetic trap. The magnetic beads of each sequence were sequentially accumulated in the magnetic trap. Opening and closing of the magnetic trap were synchronized with the fluidic workflow. Further details are given in the Results and Discussion section and in the Supporting Information, Figure S-1.

The platform consists of fluorinated ethylene propylene polymer (FEP) tubing (inner diameter 0.25 mm, outer diameter 1.60 mm, #2001001, PRO LIQUID GmbH, Germany) connected by CTFE T-junctions and union fittings (microvolume connector, 1/16 in.; 0.25 mm bore, VICI AG International, MT1CKF & MU1CKF, MACHEREY-NAGEL GmbH, Germany). Precise and programmable flow was enabled by neMESYS 290 N syringe pumps (#A3921000132, Cetoni GmbH, Germany).

Bead Extraction under Different Wetting Conditions. To compare the bead extraction in hydrophobic FEP tubes and hydrophilic glass capillaries, magnetic beads (c = 1 mg/mL) were stained with Atto-Biotin (red, #93606, Sigma-Aldrich, Germany) prior to droplet generation. To visualize the droplets, a Cy3-labeled oligonucleotide (green, Cy3-Oli3 (KK), 44 mer, #1916046, TIB Molbiol, Germany) was added to the aqueous solution; images were recorded using G-2A and Cy5-filters (four frames/s, flow rate = 1.5 μL/min).

Image and Data Analysis. The fluorescence intensities were analyzed with ImageJ (version 1.52d). Fluorescent signals were measured as the average pixel intensity for a rectangular area (region of interest, ROI). The signal slopes were fitted to
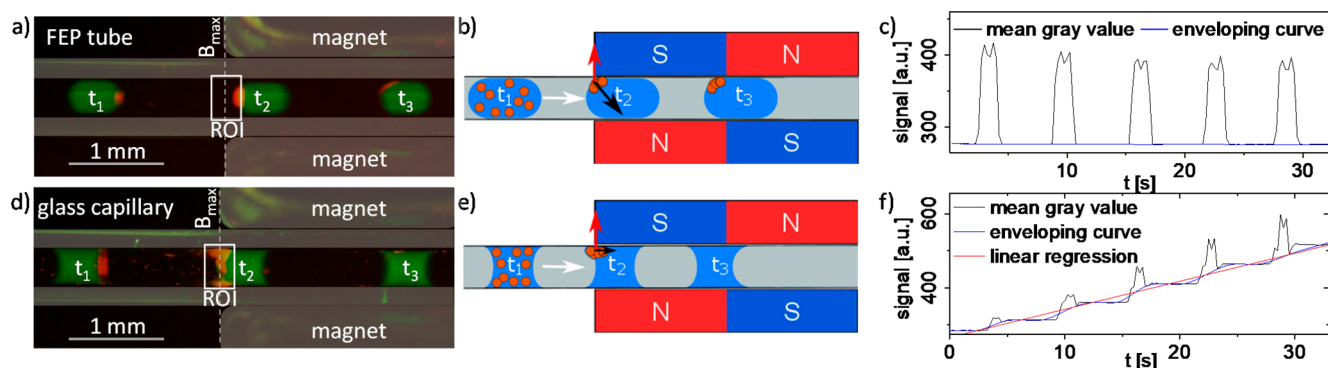
Figure 3. Magnetic bead extraction. (a,d) Attempts of magnetic bead extraction from nanoliter droplets in hydrophobic FEP tubes (a) and hydrophilic glass capillary (d) in the magnetic trap. Red, magnetic beads functionalized with Atto-Biotin. c(beads) = 1 mg/mL. White rectangle, region of interest (ROI). Dashed line, B_{max} = point of extraction. t_1, droplet before magnet. t_2, droplet at point of extraction. t_3, droplet after point of extraction. Images are overlays of multiple pictures recorded with a G-2A and a Cy5 fluorescence filter. The droplet solution was colored with a green dye (Cy3). (b,e) Illustration of (a,d). Blue, aqueous phase. Gray, carrier fluid. Brown, magnetic beads. N, magnetic north. S, magnetic south. Red arrow, magnetic force. Black arrow, capillary force. t_{1-3}, position of the same droplet at different times. (c,f) Signal intensity in the ROI (white rectangles) over time for five droplets. Black, mean gray value. Blue, enveloping curve. Red, linear regression of the accumulated signal.

the "lower enveloping curve", using the OriginPro 2019 (version 9.6.0.172) software. After plotting against the concentrations, the data was fitted by 4-Parameter logistic curves[24,25] using OriginPro 2019. Negative controls (c(target) = 0) were added as the lowest value in the dilution series.

Determination of Lower Limit of Detection (LoD). The LoD was determined as detailed in the next section. The background signal was obtained by the sigmoidal fit. The indicated concentrations were derived from the intersection with the regression curve.

Hydrophobization of Glass Capillaries. To obtain partially hydrophobic glass capillaries (2 μL minicaps, end to end, #L919.2, Hirschmann Laborgeräte GmbH & Co. KG, Germany), the capillaries were washed three times each with water, isopropanol/water (70:30, v/v), and isopropanol, and dried in a vacuum oven (60 °C) overnight. Next, the capillaries were placed upright into 200 μL PCR-tubes (781305, Brand GmbH, Germany), filled with 65 μL of a trichloro-(1H,1H,2H,2H-perfluorooctyl)silane solution (1 vol %, #448931, Sigma-Aldrich, Germany) in FC-3283. Thereby, approximately 19 mm of each capillary was filled. After 10 min at room temperature, the capillaries were washed with water and FC-3283 and dried with nitrogen. Thus, the length of the hydrophilic (untreated) part was limited to 13.2 ± 1.0 mm. As a result, the capillaries were only hydrophilic at the point of extraction.

Characterization of Light Sources. The light source emission spectra were analyzed with a blue wave spectrometer (UVN-25, 600 g/mm, #16101419, StellarNet, Inc., USA) in combination with the Cy5 ET filter set. The fiber optics of the spectrometer were focused using the 4× objective.

■ RESULTS AND DISCUSSION

Bead Extraction. The extraction of magnetic beads from a microfluidic water droplet is mainly limited by the surface tension of its interface to the surrounding carrier fluid.[14−18] To study the influence of the wetting properties of the microfluidic channels, the magnetic trap was initially operated with an unmodified hydrophobic channel (FEP tubing). We monitored the signal intensity in the region of interest (ROI). In this setup, the beads (c = 1 mg/mL) failed to penetrate the water−oil interface and remained in the droplets after passing the

predicted point of extraction at the location of B_{max} (Figure 3a and b). Therefore, the fluorescent signal reflects only the droplets passing by (Figure 3c). Thus, we conclude that this setup does not allow extracting beads at a concentration of 1 mg/mL or lower. This is in agreement with earlier studies.[10,14]

Schönberg et al.[22] have demonstrated that hydrophilic patches on the channel surface allow efficient extraction of low bead concentrations (≥1 μg/mL). In order to realize this strategy, we replaced part of the tubing by a hydrophilic glass capillary in the area of extraction. This change in the surface wetting led to an inverted shape of the aqueous droplets (Figure 3d and e) Thus, the beads no longer need to penetrate the droplet interface before they reach the channel wall and become captured. With the hydrophilic glass capillary, we observed an accumulation of the magnetic beads and consequently a linear stepwise of the fluorescence signal increase after every droplet passing the ROI (Figure 3f, and animation in Supporting Information). Clearly, the wetting of the channel facilitates the bead extraction.

For large amounts of beads, a nonlinear signal increase is observed (see Supporting Information, Figure S-2). Thus, a periodical release of the accumulated beads by removing the magnets from the channel is important. The ability to extract low amounts of beads minimizes the danger of shading and of the obstruction of the channel by the beads. The bead extraction efficiency was therefore a major limiting factor and a key concern for optimization.

Sequential Measurements. To increase the throughput, we explored the feasibility of sequential measurements. First, droplets containing 100 μg/mL streptavidin-coated beads were generated in reverse direction to flow 1 (as described above). The droplet volume was estimated to be approximately 23 nL (Supporting Information, Figure S-3). To mimic several consecutive samples, we produced a dilution series with 11 concentrations of Atto-Biotin in PBST (c = 0−10,000 pg/mL, Figure 4 a). The samples were added sequentially at the first T-junction to the droplets with the bead dispersion (details in Supporting Information, Figure S-1) resulting in about 50 droplets per sequence with a volume of approximately 43 nL. PBST was added at the second T-junction, resulting in a droplet volume of approximately 63 nL. We let the droplets incubate while moving them through a series of horizontal
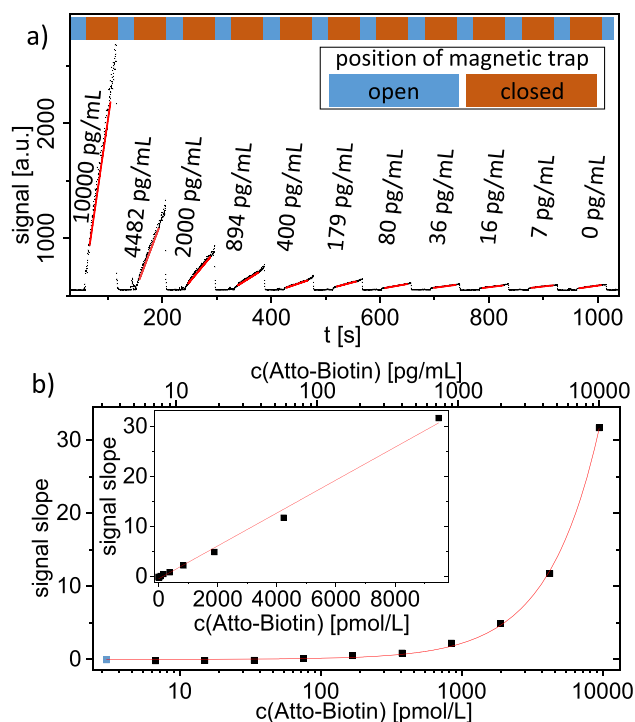
Figure 4. Sequential measurements of an Atto-Biotin dilution series. (a) Sequential measurements of 11 Atto-Biotin concentrations (0−10,000 pg/mL). The position of the magnetic trap is indicated in blue (open) and brown (closed). $n = 1$. (b) Signal slopes plotted against the different target concentrations. c(beads) = 100 μg/mL. Red, sigmoidal fit ($R^2 > 0.99$). Blue data point, negative control (0 ng/mL), added as the lowest value of the dilution series. Insert: linear scale. Red, linear fit ($R^2 > 0.99$).

coils to the magnetic trap. During the accumulation of the beads in the magnetic trap, we observed a linear signal increase for each tested concentration (Figure 4a). At the end of each sequence, the signal returned to the baseline upon each trap opening, indicative of a full release of the beads from the magnetic trap.

The signal slopes for the sequences increased proportionally with the target concentrations ($R^2 > 0.99$, Figure 4b, insert). In logarithmic plots, we used sigmoidal fits to describe the signal slope increase, as proposed earlier by Holstein et al.[24] In repeated bead accumulations, the homogeneous distribution of the magnetic beads across the droplets was tested (Supporting Information, bead distribution CV$_{slopes}$ = 5%, Figure S-4a; interassay CV$_{slopes}$ = 8%, Figure S-4b).

In summary, the linear slopes of the signals, the low signal variability, and the correlation with the different Atto-Biotin concentrations (Figure 4) indicate that droplet generation, reagent addition, and Atto-Biotin binding to the beads were accurate and reproducible in sequential measurements. Thus, we extended our system by the sequential measurement option to increase the throughput and to ensure uniform conditions for all samples of a series.

Optimization of LoD. We next evaluated and optimized the sensitivity of the microfluidic system. According to Armbruster and Pry,[26] we determined the LoD as the background signal +4 × standard deviation (SD). Thus, the LoD can be improved by reducing the background signal and/or its SD. Two major system-immanent factors were considered to increase the signal-to-background ratio: (i) the

light source, whose emission spectrum determines the fluorescence intensity by exciting the fluorescent dye and the background signal stemming from the magnetic beads and (ii) the beads as emitters of background signal, e.g., through autofluorescence and/or light scattering.

A good spectral overlap between the emission spectrum of the light source with the absorption spectrum of the fluorescent dye is a prerequisite for high fluorescence intensity. So far, our system was equipped with a metal halide lamp in combination with a Cy5 excitation filter which has its emission maximum at 593 nm (Supporting Information, Figure S-5). To increase the overlap, we replaced the metal halide lamp with an LED light source that has an emission maximum at 636 nm. The integral was 6 times higher for the LED in the range of the Cy5 filter and overlapped substantially with the absorption spectrum of the fluorescent dye (Atto-647N-Biotin, maximum absorption at 646 nm). Consequently, the LED lamp increased the slope of the dose response curve by a factor of 14. Furthermore, the signal/background ratio increased from the background for lower target concentrations. As a consequence, the use of the LED lamp improved the sensitivity of our system by more than 1 order of magnitude and reduced the LoD from about 100 pg/mL to approximately 8 pg/mL (Supporting Information, Figure S-5).

To address the beads as emitters of background signal (ii), we hypothesized that lower bead concentrations reduce the background signal. Therefore, we tested whether down titration of the magnetic beads lowers the LoD. Indeed, it was found that the magnetic bead concentration positively correlates with the background signal (Figure 5a). When evaluating the signal/background ratio, there appears to be an improvement at lower bead concentrations (Figure 5b). From this, an optimal signal/background ratio could be determined at c(beads) = 25 μg/mL. At this bead concentration, the lowest analyte concentration (2 pg/mL) can be detected at the LoD.
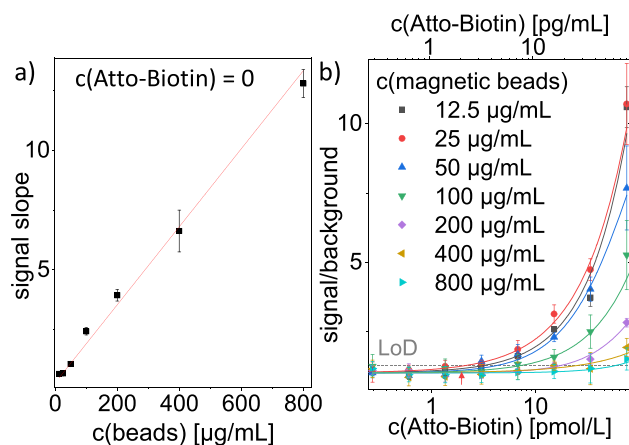

Figure 5. Enhancing the LoD. (a) Background signal measured at c(Atto-Biotin) = 0 pg/mL for a bead dilution series (800−12.5 μg/mL). Red line, linear fit ($R^2 = 0.97$). Data points, mean ± SD $n = 3$. (b) Signal/background ratio for an Atto-Biotin dilution series (0−80 and 0−400 pg/mL for c(beads) > 100 μg/mL) at different bead concentrations. Solid lines, sigmoidal fits. Dashed, LoD at c(beads) = 25 μg/mL. Red arrow, lowest detectable concentration (2 pmol/L for c(beads) = 25 μg/mL). The section of the diagram was chosen such that the differences in the area of the LoD are visible. Data for c(magnetic beads) = 100 μg/mL are reproduced from (b) (LED). Data points, mean ± SD $n = 3$.

Reducing or increasing the bead concentration results in an increase in the analyte concentration at the LoD, suggesting an ideal bead concentration of 25 μg/mL. In keeping with our findings, Teste et al.[16] have shown earlier with a comparable microfluidic setup that down titration of the bead concentration enhances the detection sensitivity. However, this study did not assess magnetic bead concentrations below 1 mg/mL, possibly because their system could not efficiently extract the magnetic beads at lower concentrations. Thus, the extraction efficiency of our system at low magnetic bead concentrations is key to enhance its sensitivity beyond earlier approaches. The capacity to detect the analyte is maintained as long as there are sufficient binding sites available.

Proof of Concept: Sandwich Immunoassays. Next, we tested the performance of our microfluidic concept with sandwich immunoassays, targeting proteins of biomedical relevance. We conducted assays for (i) the inflammatory marker interleukin 6 (IL-6)[27,28] and (ii) the metabolic master regulator mTOR (mammalian target of rapamycin), which is the central hub of the oncogenic phosphoinositide-3-kinase (PI3K)−mTOR network.[29,30] Recombinant IL-6 and mTOR were detected with antibody pairs directed against different regions of the target proteins. As the affinity of an antibody to its target is typically lower than for streptavidin−biotin ($10^{-9}-10^{-12}$ mol/L for antibodies[31] versus 10^{-13} mol/L for streptavidin−biotin[23]), the incubation time was increased from 13.5 to 27 min. Furthermore, the glass capillaries were partially hydrophobized with trichloro(1H,1H,2H,2H-perfluorooctyl)silane, as wetting of the capillary by the aqueous solution increases the risk of nonspecific protein adsorption. In the area of bead extraction, the capillaries remained hydrophilic to maintain the required wetting properties for efficient bead extraction.

The microfluidic assays were set up as pictured in Figure 1. First, a droplet train was produced, containing magnetic beads coated with the capture antibody. Samples with different concentrations of recombinant target protein were added at the first T-junction. At the second T-junction, a solution of the fluorophore-labeled antibody (detection antibody) was added. We observed for both IL-6- and mTOR-directed immunoassays a positive correlation between the signal slope and the analyte concentration (IL-6: R^2 = 0.98. mTOR: R^2 = 0.93, Figure 6, red lines). The low molecular weight protein IL-6 (20.3 kDa) was detectable at concentrations of 25 pmol/L (510 pg/mL, Figure 6a) or higher, while the high molecular weight protein mTOR (289 kDa) was detectable at a minimum concentration of 800 pmol/L (230 ng/mL) (Figure 6b). Comparable microfluidic platforms with nanoliter-reaction compartments for protein assays showed concentrations at the LoDs of 40 pmol/L (TSH-hormone, 13 kDa)[14] and 500 pmol/L (amyloid-ß peptide, 4−4.5 kDa).[18] Thus, our microfluidic setup with IL-6, which is comparable in size to TSH hormone and amyloid-ß peptide (20.3 versus 13 and 4.5 kDa, respectively), was at least 1.5−10 times more sensitive than the earlier approaches (25 versus 40 and 500 pmol/L for TSH hormone and amyloid-ß peptide, respectively).[14,18]

To the best of our knowledge, we present here the first nanoliter droplet-based microfluidic assay for mTOR. Several inherent properties of this protein can make it difficult to evaluate it in a microfluidic setup. It has been suggested that precipitation, aggregation, and/or adsorption impede the detection of proteins in microfluidics.[32] mTOR exhibits a very high molecular weight, and is membrane-associated.[33−35]
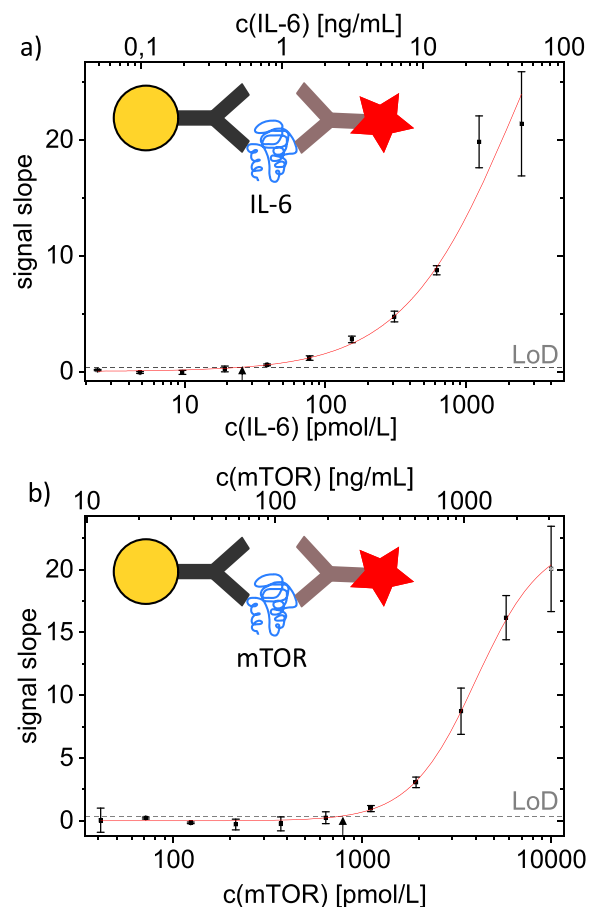
Figure 6. Microfluidic detection of proteins by a sandwich immunoassay. (a) Detection of an IL-6 dilution series (0−50 ng/mL). c(beads) = 50 μg/mL. Red, sigmoidal fit (R^2 = 0.98). Dashed line, LoD. Arrow, intersection of the sigmoidal fit and the LOD indicating the lowest detectable concentration (c(IL-6) = 25 pmol/L). Data points, mean ± SD n = 3. (b) Detection of an mTOR dilution series (0−2889 ng/mL). c(beads) = 100 μg/mL. Red, sigmoidal fit (R^2 = 0.93). Arrow, intersection of the sigmoidal fit and the LoD indicating the lowest detectable concentration (c(mTOR) = 800 pmol/L). Data points, mean ± SD n = 3.

Such properties often result in poor protein solubility, which likely explains the comparably high concentration required at the LoD for mTOR seen in this study (800 pmol/L as compared to 25 pmol/L for IL-6). Further optimization may allow lowering the detectable concentration at the LoD in the future.

■ CONCLUSION AND OUTLOOK

We present here a microfluidic platform for magnetic bead-based sandwich immunoassays in nanoliter droplets. The platform enables sequential measurements, which are key for medium and high throughput applications. By introducing a hydrophilic channel in the area of bead extraction, we achieve reliable bead extraction for bead concentrations down to 12.5 μg/mL. Earlier approaches for heterogeneous assays reported bead extraction for concentrations ≥1 mg/mL.[14,16−18,22] Thus, with this setup, the performance was improved by 2 orders of magnitude. We also show the importance of working at the optimal bead concentration, as concentrations above or below this optimum dramatically reduce the sensitivity of the system. In a proof of concept, we showed that the present platform is

compatible with immunoassays. The concentration at the LoD of the low molecular weight protein IL-6 improves by a factor of 1.5−10 compared to values reported earlier for comparable microfluidic setups.[14,17]

Conventional sandwich immunoassays, such as ELISAs on microtiter plates, typically require sample and reagent volumes of 50 µL per technical replicate, intermediate washing steps, and 2−3 incubation steps of 1−2 h each.[36] With the miniaturized analysis platform presented here, the incubation time is reduced from several hours down to 27 min. To generate approximately 50 reaction compartments at the nanoliter scale, 2 µL of sample, 1 µL of magnetic bead dispersion (c = 25−100 µg/mL), and 1 µL of detection antibody solution (c = 1 µg/mL) per sequence are sufficient. Thus, the volumes of samples and reagents are reduced by factors of 25−50. In summary, the transfer of heterogeneous immunoassays to a two-phase microfluidic system reduces the sample consumption by a factor of at least 25 while producing 50 times more technical replicates than conventional immunoassays.[36]

In the future, we envision to further develop our microfluidic platform for systems studies[37−39] to acquire data series such as time courses with high resolution and accuracy and with high numbers of biological and technical replicates. This will enhance the statistical reliability of data for computational modeling. Furthermore, we anticipate that our platform presents strong advantages where sample and/or reagent volumes are limiting and high throughput is required, such as in biomedical applications with patient material. The nanoliter reaction chambers will allow one to quantify proteins from low volumes of patient samples such as tissue or liquid biopsies. Furthermore, the high degree of parallelization enables higher accuracy, reproducibility, and time efficiency than established immunodetection methods. This is important for clinical applications that are time sensitive and require high accuracy.

In summary, the microfluidic platform presented here combines an innovative approach for efficient bead extraction from nanoliter droplets and enables sequential sandwich immunoassays. This opens new avenues for the implementation of microfluidics in the systems biology and medicine.

■ ASSOCIATED CONTENT

⒮ Supporting Information
The Supporting Information is available free of charge at https://pubs.acs.org/doi/10.1021/acs.analchem.0c00187.

Ordering details for the reagents and materials, Figures S1−S5 PDF)

Animation of the operating principle AVI)

■ AUTHOR INFORMATION

Corresponding Authors
Thomas Brandstetter − *Department of Microsystems Engineering, Chemistry & Physics of Interfaces, Albert-Ludwigs-Universität Freiburg, 79110 Freiburg im Breisgau, Baden-Württemberg, Germany;* ● orcid.org/0000-0002-3991-8295; Email: brandstetter@imtek.de

Kathrin Thedieck − *Department of Neuroscience, School of Medicine and Health Sciences, Carl von Ossietzky University Oldenburg, 26129 Oldenburg, Germany; Laboratory of Pediatrics, Section Systems Medicine of Metabolism and Signaling, University of Groningen, University Medical Center Groningen, 9713 AV Groningen, The Netherlands; Institute of Biochemistry and Center for Molecular Biosciences Innsbruck, University of Innsbruck, 6020 Innsbruck, Austria;* ● orcid.org/0000-0002-9069-2930; Email: kathrin.thedieck@uibk.ac.at, k.thedieck@umcg.nl, kathrin.thedieck@uol.de

Jürgen Rühe − *Department of Microsystems Engineering, Chemistry & Physics of Interfaces, Albert-Ludwigs-Universität Freiburg, 79110 Freiburg im Breisgau, Baden-Württemberg, Germany;* ● orcid.org/0000-0002-2534-8228; Email: ruehe@imtek.uni-freiburg.de

Authors
Lukas Metzler − *Department of Microsystems Engineering, Chemistry & Physics of Interfaces, Albert-Ludwigs-Universität Freiburg, 79110 Freiburg im Breisgau, Baden-Württemberg, Germany;* ● orcid.org/0000-0002-1984-7063

Ulrike Rehbein − *Department of Neuroscience, School of Medicine and Health Sciences, Carl von Ossietzky University Oldenburg, 26129 Oldenburg, Germany; Laboratory of Pediatrics, Section Systems Medicine of Metabolism and Signaling, University of Groningen, University Medical Center Groningen, 9713 AV Groningen, The Netherlands;* ● orcid.org/0000-0002-9104-4222

Jan-Niklas Schönberg − *Department of Microsystems Engineering, Chemistry & Physics of Interfaces, Albert-Ludwigs-Universität Freiburg, 79110 Freiburg im Breisgau, Baden-Württemberg, Germany;* ● orcid.org/0000-0002-3417-6149

Complete contact information is available at:
https://pubs.acs.org/10.1021/acs.analchem.0c00187

Author Contributions
⊥L. Metzler and U. Rehbein contributed equally.

Author Contributions
#K. Thedieck and J. Rühe contributed equally.

Notes
The authors declare no competing financial interest.

■ REFERENCES
(1) Shang, L.; Cheng, Y.; Zhao, Y. *Chem. Rev.* **2017**, *117* (12), 7964−8040.
(2) Mashaghi, S.; Abbaspourrad, A.; Weitz, D. A.; van Oijen, A. M. *TrAC, Trends Anal. Chem.* **2016**, *82*, 118−125.
(3) Seemann, R.; Brinkmann, M.; Pfohl, T.; Herminghaus, S. *Rep. Prog. Phys.* **2012**, *75* (1), No. 016601.
(4) Guo, M. T.; Rotem, A.; Heyman, J. A.; Weitz, D. A. *Lab Chip* **2012**, *12* (12), 2146−2155.

(5) Fidalgo, L. M.; Whyte, G.; Bratton, D.; Kaminski, C. F.; Abell, C.; Huck, W. T. S. *Angew. Chem.* **2008**, *120* (11), 2072−2075.

(6) Trivedi, V.; Doshi, A.; Kurup, G. K.; Ereifej, E.; Vandevord, P. J.; Basu, A. S. *Lab Chip* **2010**, *10* (18), 2433−2442.

(7) Song, H.; Chen, D. L.; Ismagilov, R. F. *Angew. Chem., Int. Ed.* **2006**, *45* (44), 7336−7356.

(8) Shembekar, N.; Chaipan, C.; Utharala, R.; Merten, C. A. *Lab Chip* **2016**, *16* (8), 1314−1331.

(9) Serra, M.; Ferraro, D.; Pereiro, I.; Viovy, J.-L.; Descroix, S. *Lab Chip* **2017**, *17* (23), 3979−3999.

(10) Rendl, M.; Brandstetter, T.; Rühe, J. *Langmuir* **2014**, *30* (43), 12804−12811.

(11) Lombardi, D.; Dittrich, P. S. *Anal. Bioanal. Chem.* **2011**, *399* (1), 347−352.

(12) Brouzes, E.; Kruse, T.; Kimmerling, R.; Strey, H. H. *Lab Chip* **2015**, *15* (3), 908−919.

(13) Gao, R.; Cheng, Z.; deMello, A. J.; Choo, J. *Lab Chip* **2016**, *16* (6), 1022−1029.

(14) Ali-Cherif, A.; Begolo, S.; Descroix, S.; Viovy, J.-L.; Malaquin, L. *Angew. Chem., Int. Ed.* **2012**, *51* (43), 10765−10769.

(15) Long, Z.; Shetty, A. M.; Solomon, M. J.; Larson, R. G. *Lab Chip* **2009**, *9* (11), 1567−1575.

(16) Teste, B.; Ali-Cherif, A.; Viovy, J. L.; Malaquin, L. *Lab Chip* **2013**, *13* (12), 2344.

(17) Ferraro, D.; Champ, J.; Teste, B.; Serra, M.; Malaquin, L.; Viovy, J.-L.; de Cremoux, P.; Descroix, S. *Sci. Rep.* **2016**, *6*, na DOI: 10.1038/srep25540.

(18) Mai, T. D.; Ferraro, D.; Aboud, N.; Renault, R.; Serra, M.; Tran, N. T.; Viovy, J.-L.; Smadja, C.; Descroix, S.; Taverna, M. *Sens. Actuators, B* **2018**, *255*, 2126−2135.

(19) Tabeling, P. *Introduction to Microfluidics*; Oxford University Press: Oxford, U.K., 2005.

(20) Rendl, M.; Brandstetter, T.; Rühe, J. *Anal. Chem.* **2013**, *85* (20), 9469−9477.

(21) Fidalgo, L. M.; Abell, C.; Huck, W. T. S. *Lab Chip* **2007**, *7* (8), 984−986.

(22) Schönberg, J.-N.; Brandstetter, T.; Rühe, J. *Procedia Eng.* **2015**, *120*, 96−99.

(23) DeChancie, J.; Houk, K. N. *J. Am. Chem. Soc.* **2007**, *129* (17), 5419−5429.

(24) Holstein, C. A.; Griffin, M.; Hong, J.; Sampson, P. D. *Anal. Chem.* **2015**, *87* (19), 9795−9801.

(25) Fong, Y.; Yu, X. *Statistics in Biopharmaceutical Research* **2016**, *8* (1), 1−11.

(26) Armbruster, D. A.; Pry, T. *Clin Biochem Rev.* **2008**, *29* (Suppl 1), S49−S52.

(27) Heinrich, P. C.; Behrmann, I.; Haan, S.; Hermanns, H. M.; Müller-Newen, G.; Schaper, F. *Biochem. J.* **2003**, *374* (1), 1−20.

(28) Mansell, A.; Jenkins, B. J. *Cytokine Growth Factor Rev.* **2013**, *24* (3), 249−256.

(29) Navas, P. R.; Thedieck, K. *Essays Biochem.* **2017**, *61* (3), 349−368.

(30) Saxton, R. A.; Sabatini, D. M. *Cell* **2017**, *168* (6), 960−976.

(31) Landry, J. P.; Ke, Y.; Yu, G.-L.; Zhu, X. D. *J. Immunol. Methods* **2015**, *417*, 86−96.

(32) Roach, L. S.; Song, H.; Ismagilov, R. F. *Anal. Chem.* **2005**, *77* (3), 785−796.

(33) De Cicco, M.; Rahim, M.; Dames, S. *Membranes (Basel, Switz.)* **2015**, *5* (4), 553−575.

(34) Betz, C.; Hall, M. N. *J. Cell Biol.* **2013**, *203* (4), 563−574.

(35) Yuan, H.-X.; Guan, K.-L. *Cancer Discovery* **2015**, *5* (11), 1127−1129.

(36) Crowther, J. R. *The ELISA Guidebook*; Walker, J. M., Ed.; Methods in Molecular Biology; Humana Press: Totowa, NJ, 2009; Vol. *516*. DOI: 10.1007/978-1-60327-254-4.

(37) Dalle Pezze, P.; Sonntag, A. G.; Thien, A.; Prentzell, M. T.; Gödel, M.; Fischer, S.; Neumann-Haefelin, E.; Huber, T. B.; Baumeister, R.; Shanley, D. P. *Sci. Signaling* **2012**, *5* (217), ra25.

(38) Dalle Pezze, P.; Ruf, S.; Sonntag, A. G.; Langelaar-Makkinje, M.; Hall, P.; Heberle, A. M.; Razquin Navas, P.; van Eunen, K.; Tölle, R. C.; Schwarz, J. J. *Nat. Commun.* **2016**, *7*, 13254.

(39) Heberle, A. M.; Razquin Navas, P.; Langelaar-Makkinje, M.; Kasack, K.; Sadik, A.; Faessler, E.; Hahn, U.; Marx-Stoelting, P.; Opitz, C. A.; Sers, C. *Life Sci. Alliance* **2019**, *2* (2), e201800257.